

# Emergent Hall phases at quantum phase transitions with accompanying changes in Fermi surface topology

N. Mohanta,<sup>1,\*</sup> S. Bandopadhyay,<sup>2</sup> S. Lal,<sup>2,†</sup> and A. Taraphder<sup>1,3</sup>

<sup>1</sup>*Department of Physics, Indian Institute of Technology Kharagpur 721302, India*

<sup>2</sup>*Department of Physical Sciences, Indian Institute of Science Education and Research 741252, India*

<sup>3</sup>*Centre for Theoretical Studies, Indian Institute of Technology Kharagpur 721302, India*

The effects of competing orders, such as superconductivity and ferromagnetism, on a Fermi liquid are well established. A comprehensive understanding of such a competition in a metal whose Fermi surface has a non-trivial topology is yet to be achieved. Here, we address this question in a prototypical system: the 2D Rashba semimetal<sup>1</sup>. We show that dominant superconductivity interplays with Rashba spin orbit interactions (SOI) in forming a novel intrinsic anomalous Hall effect (AHE) with gapless edge states of Bogoliubov-de Gennes (BdG) quasiparticles. As in the case of itinerant ferromagnets<sup>2</sup>, the intrinsic AHE arises from Berry curvature effects in the band structure. This phenomenon is robust even as subdominant ferromagnetism dramatically changes the nature of pairing symmetry<sup>6,7</sup>. An emergent spin Hall phase involving a change in Fermi surface topology is found to accompany this quantum phase transition. We demonstrate the coexistence of the original and novel AHE in the presence of weak disorder. We offer a comparison of our results with experiments on the two dimensional electron gas at oxide hetero-interfaces<sup>8,9</sup> as well as make some testable predictions.

AHE has been observed in wide variety of materials<sup>2</sup> such as complex oxide ferromagnets<sup>10–13</sup>, ferromagnetic semiconductors<sup>5</sup>, spinels<sup>14,15</sup>, Heusler alloys<sup>16,17</sup>, layered dichalcogenides<sup>18</sup> etc. The intrinsic mechanism for the AHE originates due to spin-orbit interaction (SOI) in parity-broken itinerant ferromagnets and is understood in terms of the Kurlus-Luttinger semi-classical theory<sup>19</sup>. More recently, the intrinsic AHE has been explained as a topological mechanism: electrons at the Fermi surface can acquire a Berry phase from the existence of magnetic monopoles in momentum space arising from a non-trivial topology of electronic bands<sup>3–5</sup>. There are extrinsic contributions to the anomalous Hall conductivity (AHC), such as side-jump<sup>20</sup> or skew-scattering from impurities<sup>21</sup>, which sometimes dominate over the intrinsic process<sup>22</sup>.

A particularly simple model for the intrinsic AHE is the two-dimensional ferromagnetic Rashba model<sup>23</sup>. Here also, the AHE appears due to a Berry phase picked up at the avoided band-crossing induced by Rashba SOI (see Fig.1(a) and (b)). The AHC  $\sigma_{xy}$  takes a finite value and is proportional to the Berry phase (in units of  $e^2/h$ ) when there is a gap at the Fermi level at the avoided band-crossing point<sup>24</sup>. However, an additional singlet superconducting pairing gap at the Fermi level

will suppress the magnetization induced gap responsible for stabilizing the AHE. This leads us to expect a clear suppression of the intrinsic AHE by the singlet superconductivity.

In this paper, we study the intrinsic AHE of BdG quasiparticles in two-dimensional  $s$ -wave superconductors with Rashba SOI and ferromagnetism based on a self-consistent mean-field solution of the pairing gap. The system is modeled by the following Hamiltonian

$$\mathcal{H} = \sum_{k,\sigma} \epsilon_k c_{k\sigma}^\dagger c_{k\sigma} + \alpha \sum_{k,\sigma,\sigma'} (\mathbf{g}_k \cdot \boldsymbol{\sigma})_{\sigma\sigma'} c_{k\sigma}^\dagger c_{k\sigma'} - m_z \sum_{k,\sigma,\sigma'} \sigma_{\sigma\sigma'}^z c_{k\sigma}^\dagger c_{k\sigma'} + \sum_k (\Delta c_{k\uparrow}^\dagger c_{-k\downarrow}^\dagger + h.c.) \quad (1)$$

where  $\epsilon_k = -2t(\cos k_x + \cos k_y) - \mu$  represents the dispersion of electrons,  $t$  the hopping parameter,  $\mu$  the chemical potential,  $m_z$  the magnetization perpendicular to the two-dimensional plane,  $\alpha$  the strength of Rashba SOI and  $\mathbf{g}_k = (\sin k_y, -\sin k_x)$ .  $\Delta = -\langle c_{k\uparrow} c_{-k\downarrow} \rangle$  is the superconducting pairing gap.

We briefly recall that for the case of a vanishing magnetization and  $s$ -wave superconductivity, the Rashba SOI leads to a cusp-like feature at the  $(k_x = \pm\pi, k_y = \pm\pi)$  points in the electronic bands; the emergent electronic excitations around this cusp correspond to massless Dirac fermions<sup>1</sup> with a Berry phase  $\gamma = \pi$  (see Fig.1(a)). This gives rise to two edge currents in the system with opposite helicities, in turn giving a universal negative value of the intrinsic spin Hall conductivity (SHC) while the intrinsic AHC vanishes due to an exact cancellation. A finite superconducting order parameter will open a gap in the quasi-particle spectrum at the Fermi surface, leading to an avoided band-crossing at the cusp. This gives mass to the Dirac fermions, leading to a Berry phase for the BdG quasiparticles  $\gamma < \pi$  (see Fig.1(b)). It is expected that this Berry-phase contribution to the SHC remains finite in the presence of a superconducting order parameter<sup>25</sup>. It is also illuminating to write the pairing in the helicity basis favoured by the Rashba SOI: pairing within a band of a given helicity has chiral  $p$ -wave pairing symmetry ( $p_x \pm ip_y$ ) while inter-helicity band pairing possesses  $s$ -wave symmetry. This can be seen as follows. The energy bands created by the Rashba SOI and the magnetization are given by  $\epsilon_\pm(\mathbf{k}) = \epsilon_k \pm \xi$ , where  $\xi = (\alpha^2 |\mathbf{g}_k|^2 + m_z^2)^{1/2}$  and the corresponding eigenstates  $[c_{k,+}, c_{k,-}]$  are obtained by the following transformation

$$\begin{pmatrix} c_{k\uparrow} \\ c_{k\downarrow} \end{pmatrix} = \frac{1}{\sqrt{2}} \begin{pmatrix} a_1 & b_1 e^{i\phi} \\ a_2 e^{-i\phi} & b_2 \end{pmatrix} \begin{pmatrix} c_{k,+} \\ c_{k,-} \end{pmatrix} \quad (2)$$

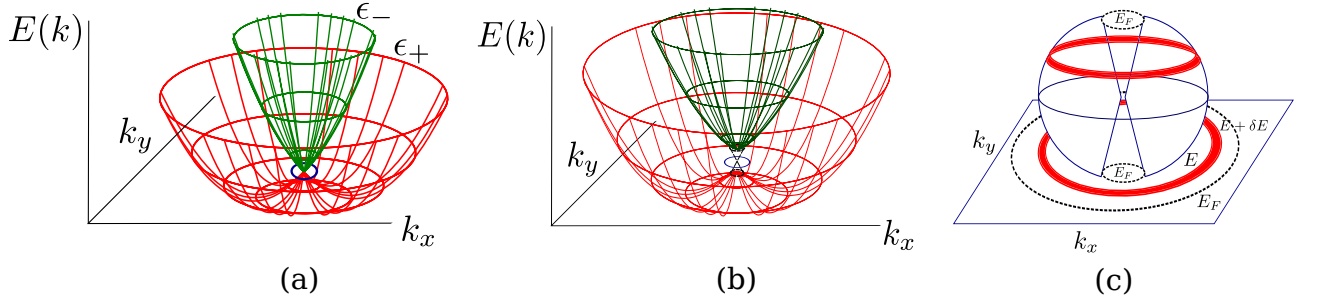


FIG. 1. (Color online) (a) The band structure for the 2D Rashba semimetal. A cusp-like feature connects the two bands  $\epsilon_+$  and  $\epsilon_-$ , with a Dirac-like dispersion of the electrons. The blue circle displays a non-contractible loop around the Dirac point, with a non-trivial topology of the Fermi surface characterized by a Berry phase  $\gamma = \pi$  (for the lower band). (b) The opening of a gap leads to a mass for the Dirac-like electronic excitations. The gap can arise due to a finite superconducting order parameter or magnetization. The black, dashed Dirac cone connecting the upper and lower bands signifies the gapless edge-states present in any finite system. These edge states are again surrounded by a non-contractible loop leading to a Berry phase  $\gamma < \pi$ , and make the system a Anomalous Hall insulator with topological properties. (c) A stereographic projection of the energy contours on the  $(k_x, k_y)$  plane onto a sphere touching the plane at its south pole. The black dashed line projects the Fermi energy onto a latitude near the North pole, while states with energies in the interval  $E$  to  $E + \delta E$  (red band) are projected onto the northern hemisphere as shown. A finite superconducting order parameter connects the upper boundary with the south pole, making it topologically equivalent to a ring torus.

where  $\phi = \tan^{-1}(\sin k_x / \sin k_y)$ ,  $a_1 a_2 = b_1 b_2 = -\alpha |\mathbf{g}_k| / (2\xi)$  and  $a_1 b_2 - b_1 a_2 = m_z / \xi$ . When written in the quasi-particle basis  $[c_{k,+}, c_{k,-}]$ , Hamiltonian (1) reduces to

$$\mathcal{H} = \sum_{\mathbf{k}} [\epsilon_+(\mathbf{k}) c_{k,+}^\dagger c_{k,+} + \epsilon_-(\mathbf{k}) c_{k,-}^\dagger c_{k,-} + \Delta_\pm c_{k,\pm}^\dagger c_{-k,\pm}^\dagger + \Delta_s c_{k,+}^\dagger c_{-k,-}^\dagger + h.c.] \quad (3)$$

where  $\Delta_\pm = (-\alpha |\Delta| / (2\xi)) (\sin k_y \pm i \sin k_x)$  and  $\Delta_s = m_z |\Delta| / \xi$  are, respectively, the intra-band and inter-band pairing amplitudes. Evidently,  $\Delta_\pm$  has chiral  $p$ -wave pairing symmetry whereas  $\Delta_s$  is of  $s$ -wave symmetry. As shown in Fig.(1(c)), a stereographic projection of the energy contours on the  $(k_x, k_y)$  plane onto a sphere show that a finite superconducting order parameter turns the sphere into a ring torus.

Any finite magnetization in the system causes an imbalance in the spin populations of the BdG quasiparticles by introducing a Zeeman splitting between the helicity bands. Increasing the magnetization from zero also leads to a gradual closing of the avoided band-crossing at the  $(k_x = \pm\pi, k_y = \pm\pi)$ -points near the Fermi level. This gives, in turn, an increase in the Berry curvature and thence the AHC from the neighbourhood of the  $(k_x = \pm\pi, k_y = \pm\pi)$  points. This can be seen by writing the Hamiltonian (1) in the Nambu-spin basis  $\Psi = [\psi_k, \psi_{-k}^\dagger]$ , where  $\psi_k = [c_{k\uparrow}, c_{k\downarrow}]$ , as

$$H(\mathbf{k}) = \begin{pmatrix} \epsilon_k - h_z \sigma_z + \alpha \mathbf{g}_k \cdot \boldsymbol{\sigma} & i\Delta \sigma_y \\ -i\Delta \sigma_y & -\epsilon_k + h_z \sigma_z + \alpha \mathbf{g}_k \cdot \boldsymbol{\sigma}^* \end{pmatrix} \quad (4)$$

From this, we obtain the quasi-particle spectrum

$$E(\mathbf{k})_\pm = \pm(\epsilon_k^2 + \xi^2 + \Delta^2 \pm 2\sqrt{\Delta^2 m_z^2 + \epsilon_k^2 \xi^2})^{1/2}, \quad (5)$$

The quasi-particle spectrum for various values of the magnetization  $m_z$  is shown in FIG. 2.

When the chemical potential  $\mu$  is inside the gap induced by the avoided band-crossing, the Berry curvature  $\Omega$  and Berry phase  $\gamma$  picked up due to the lower band (with  $p_x + ip_y$ -wave pairing) is given by

$$\Omega = \frac{m_z^2 \alpha^2 |\Delta|^2 \epsilon_+ \cos k_x \cos k_y}{2\xi(\epsilon_+^2 + \Delta_+ \Delta_-)^{3/2}}, \quad \gamma = \frac{1}{2\pi} \iint_{B.Z.} d^2 \vec{k} \Omega(\vec{k}) \quad (6)$$

The AHC is obtained as  $\sigma_{xy} = \frac{e^2}{2h} \gamma$ <sup>24,26</sup>. The Berry phase contribution from the other BdG bands (whose pairing is  $p_x - ip_y$ -wave) is suppressed by the magnetization induced energy separation between the BdG bands of opposite helicity. In Fig. 3, the pairing amplitude  $\Delta_+$  and the Berry curvature  $\Omega$  are shown in the first BZ for various magnetization  $m_z$ .  $\Delta_+$  has nodal structure due to the Rashba SOI, while  $\Omega$  shows finite value near the Fermi level. Further, the change in the topology of the band structure in the neighborhood of the  $(k_x = \pm\pi, k_y = \pm\pi)$ -points is shown in the lower panel of Figure(2): the effects of the competition between gaps induced by  $\Delta$  and  $m_z$  are seen to change the topology of the BdG bands nearest to the superconducting gap.

We stress that the AHE, under consideration, is different from that obtained in the ferromagnetic Rashba model<sup>23</sup>: the gap at the Fermi level in the latter is opened by Zeeman splitting whereas in the former, the pairing gap serves the same purpose. Precisely at a critical value of the magnetization given by  $m_z^* = \sqrt{\Delta^2 + \mu^2}$ , where  $\Delta$  is the superconducting order parameter and  $\mu$  the chemical potential, we find massless Dirac fermions associated with an emergent SHE of the BdG quasiparticles. This can be seen in Fig.(2) with  $m_z^*(\mu = 0) = \Delta$ , as well as from the effective low-energy Hamiltonian in the neighbourhood of  $m_z^*$

$$H_+(\mathbf{k}) = (v \sin k_y) \sigma_x + (v \sin k_x) \sigma_y + (m_z^* - m_z) \sigma_z \quad (7)$$

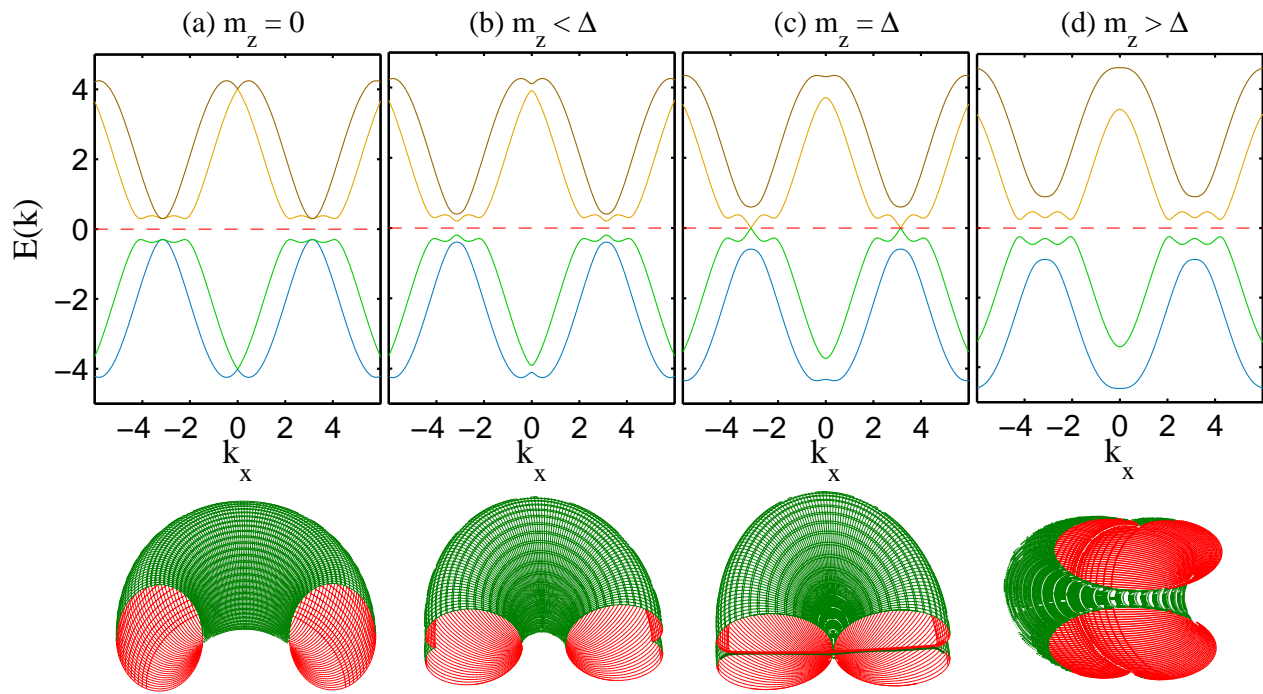


FIG. 2. (Color online) The quasi-particle spectra for various values of the magnetization  $m_z$  with constant parameters  $\mu = 0$ ,  $\Delta = 0.3$ ,  $\alpha = 1.0$  and  $t = 1$ . The avoided level-crossings near  $k_x = \pm\pi$  points at the Fermi-level give rise to finite Berry-phase  $\gamma$  leading to an AHE in the quasi-particle bands. Furthermore, as  $m_z$  increases, the quasi-particle excitation gap reduces and becomes zero at  $m_z^* = \Delta = 0.3$  (at  $k_x = \pm\pi$  in column (c)). With further increase of  $m_z$ , a new excitation gap, proportional to Rashba SOI, opens up (column (d)) and the system undergoes a transition from topologically trivial to non-trivial superconductor. Figures in lower panel describe the topology of the two BdG bands nearest the superconducting gap in the neighborhood of the  $(k_x = \pm\pi, k_y = \pm\pi)$ -points through the stereographic projection method described in Fig(1(c)). (a) As shown in Fig(1(c)), a finite superconducting order parameter turns the sphere into a ring torus by connecting its upper and lower boundaries. The effects of a competing incipient uniform magnetization can then be studied by considering its effects on the equatorial plane. (b) A finite magnetization gradually closes the gap defining the ring torus by uniformly pinching it on the equatorial plane. For a sub-dominant magnetization  $m_z < m_z^*$ , the inner hole of the ring torus is still dependent on the SC order parameter. (c) At  $m_z = m_z^*$ , the inner hole due to the superconductivity closes and the resulting topology is that of a Horn Torus which is pinched from two orthogonal directions. This change in the topology of the torus signals the quantum phase discussed above, coinciding with the emergent spin Hall phase. (d) For  $m_z > m_z^*$ , the topology is once again that of a ring torus, but whose inner hole is now dependent on the magnetization.

where the effective velocity of the emergent Dirac quasi-particles is given by  $v = \alpha (1 - \frac{\mu^2}{m_z m_z^*})^{1/2}$ . The mass of these quasiparticles is clearly seen to vanish at  $m_z = m_z^*$ . It is important to note that this effective low-energy subspace is formed out of two admixtures involving all four quasiparticle bands. The anomalous Hall and spin Hall conductivities computed for this system with a fixed  $\Delta = 0.1$ ,  $\mu = 0$  and with varying  $m_z$  is shown in Fig. 4(a).

As shown in the mean-field phase diagram Fig. 4(b), the emergent SHE is concomitant with a quantum phase transition from normal superconductivity to topological superconductivity due to the dramatic change in pairing symmetry in the presence of Rashba SOI<sup>6,7</sup>. This is understood by noting that, upon tuning the magnetization in the regime  $0 < m_z < m_z^*$ , one of the helicity-bands is pushed away from the superconducting gap edge, and the inter-band s-wave pairing is thus strongly suppressed. For  $m_z > m_z^*$ , this leads the system into a phase taken to be a canonical example of topological superconductivity: a superconducting state with spinless  $p_x + ip_y$ -wave

pairing belonging to the effective low-energy Hamiltonian

$$H_+(\mathbf{k}) = \begin{pmatrix} \epsilon_+ & \Delta_+ \\ \Delta_+^* & -\epsilon_+ \end{pmatrix}. \quad (8)$$

Thus, beyond  $m_z^*$ , the quasi-particle gap is opened instead by the magnetization and Rashba SOI<sup>27</sup>, leading to an intrinsic AHE which coexists with topological superconductivity. In this way, we find that the intervening SHE at the quantum critical point is correlated with the change in the momentum-space topology of the BdG quasiparticles shown in the lower panel of Fig. 2.

While the results, presented here, are robust for the case of a proximity-effect induced singlet superconducting pairing, we employ a self-consistent BdG formalism for the case when the pairing originates from an intrinsic superconducting instability of the 2D electronic system. Here, the Hamiltonian (1) is diagonalized via a spin-generalized Bogoliubov-Valatin transformation  $\hat{c}_{k\sigma} = \sum_{n\sigma'} u_{n\sigma\sigma'}(\mathbf{k})\hat{\gamma}_{n\sigma'} + v_{n\sigma\sigma'}^*(\mathbf{k})\hat{\gamma}_{n\sigma'}^\dagger$ , where  $u_{n\sigma\sigma'}(\mathbf{k})$  and  $v_{n\sigma\sigma'}(\mathbf{k})$  are quasi-particle and quasi-hole amplitudes re-

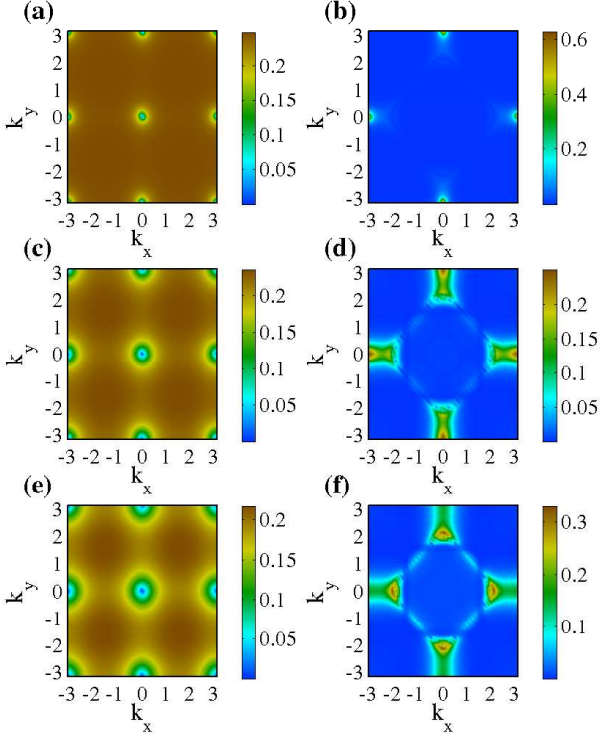


FIG. 3. (Color online) Momentum-space plots of the superconducting pairing amplitude  $|\Delta_+|$  (left column) and the Berry curvature  $\gamma$  (right column) for  $m_z = 0.2$  in (a)-(b),  $m_z = 0.5$  in (c)-(d) and  $m_z = 0.8$  in (e)-(f). Other parameters:  $\mu = 0$ ,  $\Delta = 0.5$ ,  $\alpha = 1.0$  and  $t = 1$ .  $\Delta_+$  has the nodal structure as the Rashba SOI but  $\gamma$  takes finite value only at the avoided level-crossing at Fermi level in the quasi-particle spectrum.

spectively and  $\hat{\gamma}_{n\sigma'}$  is a Fermionic operator. The mean-field pairing amplitude  $\Delta = -U \langle c_{k\uparrow} c_{-k\downarrow} \rangle$ , where  $U$  is the pairwise attractive interaction potential is obtained via the Bogoliubov amplitudes  $u_{n\sigma}(\mathbf{k})$  and  $v_{n\sigma}(\mathbf{k})$  ( $\sigma'$ , being a pseudo-index, is omitted for simplicity) as

$$\Delta(\mathbf{k}) = -U \sum_n [u_{n\uparrow}(\mathbf{k})v_{n\downarrow}^*(-\mathbf{k})(1 - f(E_n)) + u_{n\downarrow}(\mathbf{k})v_{n\uparrow}^*(-\mathbf{k})f(E_n)] \quad (9)$$

where  $f(x) = 1/(1 + e^{x/(k_B T)})$  is the Fermi function at temperature  $T$  and  $k_B$  is the Boltzmann constant.

In FIG. 5(a),(c) and (e) the variations of  $|\Delta_+|$  and  $|\sigma_{xy}|$  and  $|\sigma_{xy}^{2DEG}|$  (anomalous Hall conductivity for Ferromagnetic-2DEG with Rashba SOI) with Rashba SOI for various  $m_z$  is shown. Interesting, both  $|\Delta_+|$  and  $|\sigma_{xy}|$  reveal non-monotonic behaviour with respect to increasing Rashba SOI strength  $\alpha$ . This is because, with large  $\alpha$ , the enhanced rate of spin-precession due to Rashba SOI acts as a dephasing mechanism for the superconducting pairing thus reducing the pairing amplitude  $\Delta$ . Also, this non-monotonic behaviour is the striking difference from the AHE in Ferromagnetic-2DEG with Rashba SOI (shown in Fig. 5(e)). A point-contact Andreev-tunneling spectroscopy can be used to probe

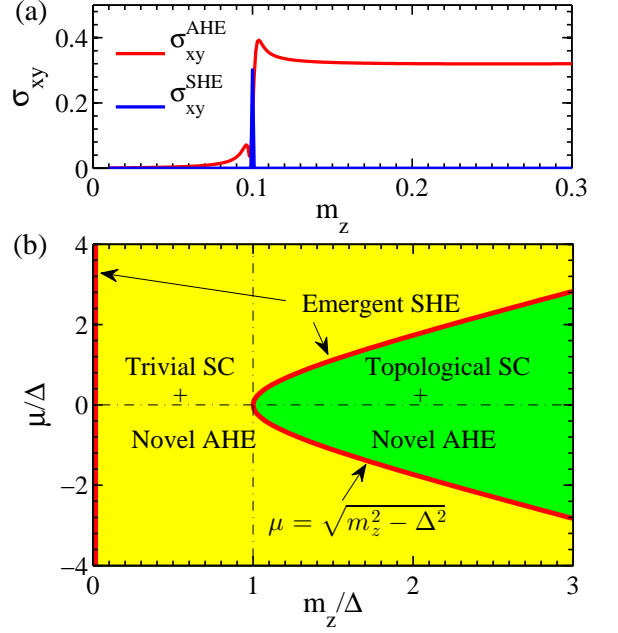


FIG. 4. (Color online) (a) The variation of the anomalous Hall conductivity  $\sigma_{xy}^{AHE}$  and the spin-Hall conductivity  $\sigma_{xy}^{SHE}$  with magnetization  $m_z$  for  $\Delta = 0.1$  and  $\mu = 0$ .  $\sigma_{xy}^{SHE}$  shows a delta-function like peak only at  $m_z = m_z^*$ . (b) Phase diagram showing the appearance of different Hall phases and the superconductivity. It is evident that the emergent SHE will appear only at  $m_z = 0$  and along the critical points defined by  $\mu = \sqrt{m_z^2 - \Delta^2}$  line. On both the topologically trivial (yellow region) and non-trivial (green region) superconducting phases, the novel AHE is present.

this new type of AHE in Rashba-coupled superconductor. On the other hand, both  $|\Delta_+|$  and  $|\sigma_{xy}|$  are seen to decrease with increasing  $m_z$  as in FIG. 5(b) and (d). This is due to the fact that both the quantities depend explicitly on the pairing gap  $\Delta$ , and a self-consistent treatment of  $\Delta$  reveals that it decreases with an increasing  $m_z$  due to pair-breaking processes. The anomalous hall conductivity  $|\sigma_{xy}^{2DEG}|$  decreases very slowly with  $m_z$  (shown in Fig. 5(f)) because with increasing the gap at Fermi level, the Berry curvature reduces at very slow rate. The variations of the pairing gap  $\Delta_+$  and AHC  $\sigma_{xy}$  with the chemical potential  $\mu$  are shown in FIG. 5(g)-(h). The pairing exists over a large filling range but the AHC is peaked near the avoided level-crossings only.

The nature of the variation of  $|\Delta_+|$  with respect to the Rashba SOI ( $\alpha$ ) can shed light on the non-monotonic behaviour of superconductivity observed at LaAlO<sub>3</sub>/SrTiO<sub>3</sub> interface<sup>8,9</sup>. In this Oxide interface, superconductivity ( $T_c \simeq 200$  mK) is observed at very low-filling and the phase diagram is traced by varying the gate-voltage ( $V_{bg}$ ) which controls both the electron-concentration ( $n_{2D}$ ) and the Rashba spin-orbit splitting ( $\Delta_{so}$ ). With increasing  $n_{2D}$ , the Curie temperature ( $T_c$ ) should reveal a dome-shaped superconducting phase in the  $n_{2D} - T_c$ -space. However, the enhanced  $\Delta_{so}$  serves as a pair-breaking agent to kill the superconductivity as  $V_{bg}$  is increased. The competition between these two op-

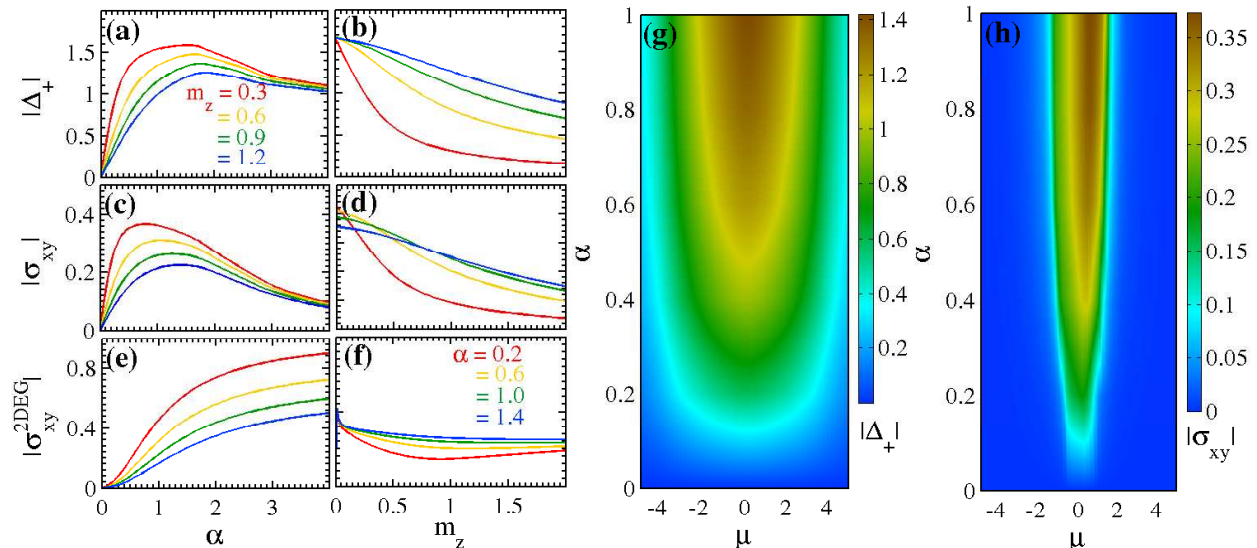


FIG. 5. (Color online) Figures (a)-(f) shows the variation of the pairing amplitude  $|\Delta_+|$  and AHC  $|\sigma_{xy}|$  and  $|\sigma_{xy}|^{2DEG}$  (in units of  $e^2/(2h)$ ) with magnetization  $m_z$  and Rashba SOI  $\alpha$  with  $\mu = 0$ ,  $U = 2.0$  and  $t = 1$ . The non-monotonic feature of  $|\sigma_{xy}|$  (Fig. (c)) distinguishes the novel AHE from the conventional AHE observed in ferromagnetic Rashba model without superconductivity. On the other hand, both  $|\Delta_+|$  and AHC  $|\sigma_{xy}|$  decays monotonically due to the explicit dependence in  $\Delta$  which reduces with increasing  $m_z$  in the self-consistent calculation. Please note that, in Fig.(d),  $|\sigma_{xy}|$  is valid except at  $m_z = 0$  where the time-reversal symmetry is intact and we get an emergent SHE. Figures (g) and (h) are the plots of the pairing amplitude  $|\Delta_+|$  and AHC  $|\sigma_{xy}|$  (in units of  $e^2/(2h)$ ) in the  $\mu - \alpha$ -plane for constant  $U = 2.0$ ,  $h_z = 0.5$  and  $t = 1$ . This shows that although superconductivity can be in a large filling-range, the AHE appears only within a narrow window of filling.

positive effects of  $n_{2D}$  and  $\Delta_{so}$  on superconductivity, with increasing  $V_{bg}$ , a non-monotonic feature is observed.

Real systems, such as two-dimensional superconducting films, are always encumbered with various kinds of imperfections which may, sometimes, be magnetic in nature. Also, the AHE that we study here, is born out of a superconductor which shows fascinating behaviours in presence of disorder. It is, therefore, interesting to analyze the nature of the AHE and its coexistence with the topological superconductivity in the disordered situation. The topological superconductivity is Rashba SOI-generated and non-local. In the disordered regime one has to take recourse to the real-space version of it. We shall investigate order-parameters like pairing gap or magnetization and connect with the novel-AHE and its possible coexistence with other orders.

The usual BCS superconductor is robust against weak non-magnetic disorder<sup>28</sup>. However, sufficiently large disorder can drive the system to a non-superconducting one<sup>29</sup>. We introduce the non-magnetic disorder as a local shift in the chemical potential and the consequent Hamiltonian is  $H_{non-mag} = \sum_{i\sigma} V_d c_{i\sigma}^\dagger c_{i\sigma}$ , where  $V_d$  is the random disorder potential which varies within  $[-W, W]$ ,  $W$  being the maximum strength of the disorder. The conventional route to study disordered superconductivity is to solve the self-consistent BdG equations  $\mathcal{H}\phi_n(r_i) = \epsilon_n\phi_n(r_i)$  where  $\phi_n = [u_{n\uparrow}(r_i), u_{n\downarrow}(r_i), v_{n\uparrow}(r_i), v_{n\downarrow}(r_i)]$  at every site using Bogoliubov transformation  $\hat{c}_{i\sigma}(r_i) = \sum_{i,\sigma'} u_{n\sigma\sigma'}(r_i)\hat{\gamma}_{n\sigma'} + v_{n\sigma\sigma'}^*(r_i)\hat{\gamma}_{n\sigma'}^\dagger$ . As above, the mean field pairing amplitude  $\Delta(r_i) = -U \langle c_{i\uparrow}c_{i\downarrow} \rangle$  and mag-

netization  $m(r_i) = \langle c_{i\uparrow}^\dagger c_{i\uparrow} - c_{i\downarrow}^\dagger c_{i\downarrow} \rangle$  are calculated from the following relations:

$$\Delta(r_i) = -U \sum_n [u_{n\uparrow}(r_i)v_{n\downarrow}^*(r_i)(1 - f(E_n)) + u_{n\downarrow}(r_i)v_{n\uparrow}^*(r_i)f(E_n)] \quad (10)$$

$$m(r_i) = \sum_{n,\sigma} u_{n\uparrow}^* u_{n\downarrow} f(E_n) + v_{n\uparrow} v_{n\downarrow}^* (1 - f(E_n)) \quad (11)$$

FIG. 6 represents the spatial profile of superconductivity and ferromagnetism in the two-dimensional plane. In the highly disordered situation, these two competing orders stay apart in spatially excluded regions<sup>30</sup>. It is therefore inferred that, the usual AHE, which is observed in ferromagnetic Rashba model, resides in the ferromagnetic regions and on the other hand, the novel AHE exists in the superconducting islands. In this way, a spatial phase separation enables the two types of AHE to coexist while being microscopically apart. When the Rashba SOI and Zeeman field is large enough to convert the ordinary superconductivity into a topological one, the resulting topological superconductivity would be more vulnerable to non-magnetic impurity scattering due to explicitly broken time-reversal symmetry<sup>31</sup>.

Magnetic impurity, on the other hand, has detrimental effects on s-wave superconductors. The interaction between the magnetic impurity and the itinerant electrons can be represented by the Hund's coupling-like term  $\hat{H}_{mag} = -J_H \sum_j \vec{S}_j \cdot \vec{s}_j$ , where  $\vec{S}_j$  is the impurity spin and  $\vec{s}_j = \frac{1}{2} c_{j\sigma}^\dagger \vec{\sigma}_{\sigma\sigma'} c_{j\sigma'}$  represents the intrinsic

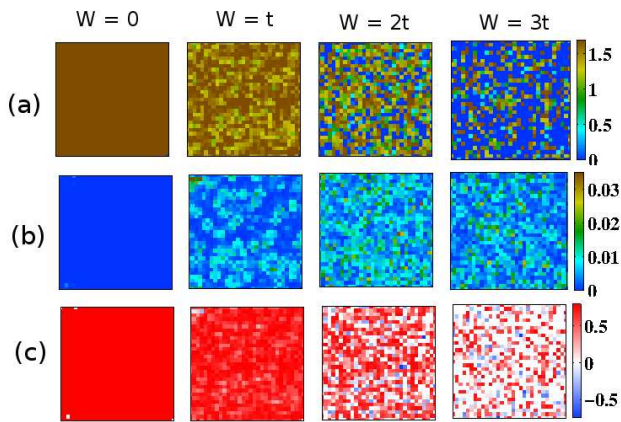


FIG. 6. (Color online) The spatial distribution of the local pairing amplitude  $|\Delta(r_i)|$  (top row) and magnetization (middle row) in  $31 \times 31$  square lattice. The columns are for disorder strength  $W = 0, t, 2t$  and  $3t$  (from left to right). The lowest row shows the spatial profile of the dominating order; red and blue colours represent regions of superconductivity and ferromagnetism. The parameters used are  $U = -1$ ,  $h_z = 0.5$  and  $\alpha = 0.8$ .

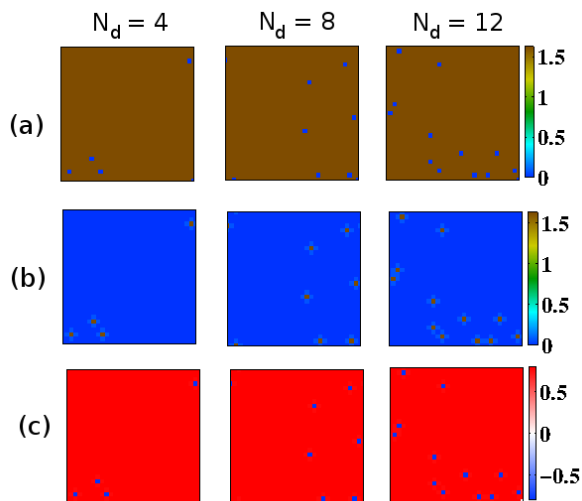


FIG. 7. (Color online) The spatial distribution of the local pairing amplitude  $|\Delta(r_i)|$  (top row) and magnetization (middle row). The columns are for different number of magnetic impurity  $N_d = 4, 8$  and  $12$  (from left to right). The lowest row shows the spatial profile of the dominating order; red and blue colours represent regions of superconductivity and ferromagnetism. The parameters used are  $U = -1$ ,  $J_H = 1$  and  $\alpha = 0.8$ .

sic electron spin. Assuming the impurity to be represented by a classical spin of unit amplitude and polar angles  $\theta$  and  $\phi$ , we have, at the mean-field level,  $\hat{H}_{mag} = -(J_H/2) \sum_j \Psi_j^\dagger \Pi \Psi_j$ , where  $\Psi_j$  is the two-component

spinor and  $\Pi = (\sin \theta \cos \phi) \sigma_x + (\sin \theta \sin \phi) \sigma_y + (\cos \theta) \sigma_z$ . If we assume that the impurity spin is aligned perpendicular to the 2D-plane (*i.e.*,  $\theta = 0$ ), we obtain  $\hat{H}_{mag} = -J_H/2 \sum_{j, \sigma, \sigma'} \sigma_{\sigma\sigma'}^z c_{j\sigma}^\dagger c_{j\sigma'}$ , where  $j$  runs over  $N_d$  number of impurity sites, randomly located in the two-dimensional space. As shown in FIG. 7, superconductivity is totally destroyed at the impurity sites and we again have the spatial separation of superconductivity and ferromagnetism. As in the case of non-magnetic disorder, here also the two types of AHE coexist. The conventional AHE resides at the impurity sites and the novel AHE at the superconducting regions.

To summarize, we have proposed a novel AHE of BdG quasiparticles which arises from an interplay of singlet superconducting pairing and a finite perpendicular magnetization in presence of Rashba SOI. At a critical magnetization, an emergent spin Hall phase is found to coincide with a transition from normal to topological superconductivity. At yet larger magnetization, the topological superconductivity coexists with the AHE. For the case when superconductivity is suppressed completely by magnetization, we expect a first order phase transition into an emergent intrinsic AHE phase of the ferromagnetic 2DEG Rashba model. We observed non-monotonic behaviour of the AHC with respect to the Rashba SOI strength due to the fact that at very large SOI, the enhanced spin-precession is pair-breaking for superconductivity. In this connection, we explain the non-monotonic feature of superconductivity observed at  $\text{LaAlO}_3/\text{SrTiO}_3$  interface when gate-voltage is tuned. The non-monotonic dependence of the AHC on Rashba SOI in the presence of a superconducting order parameter can be easily distinguished from that obtained in its absence. The coexistence of superconductivity and the AHE is also expected to lead to a subtle interplay between Andreev reflection and Hall conductivity of edge-state BdG quasiparticles in several of these phases. For concreteness, we have studied the effects of disorder in this model-system and found that both magnetic and non-magnetic disorder result in a co-existence of the novel AHE with the conventional AHE, observed in ferromagnetic Rashba model. The scenario presented here can be observed in thin superconducting film or superconducting 2DEG at Oxide interfaces and semiconducting hetero-structures with Rashba SOI.

*Note added: During the preparation of this manuscript, a work on AHC in similar systems appeared on the arxiv (arXiv:1407.3883).*

N.M. acknowledges MHRD, India for support. S.L. gratefully acknowledges support from the DST, Govt. of India through a Ramanujan fellowship. S.B. and S.L. thank CTS, IIT-Kharagpur for hospitality while a part of the work was conducted. S.B. and S.L. thank Anirban Mukherjee for invaluable help with visualizing the Fermi surface topology diagrams.

- 
- \* nmohanta@phy.iitkgp.ernet.in  
† slal@iiserkol.ac.in
- <sup>1</sup> J. Sinova *et al.*, Phys. Rev. Lett. **92**, 126603 (2004).
  - <sup>2</sup> N. Nagaosa, J. Sinova, S. Onoda, A. H. MacDonald, and N. P. Ong, Rev. Mod. Phys. **82**, 1539 (2010).
  - <sup>3</sup> Z. Fang *et al.*, Science **302**, 92 (2003).
  - <sup>4</sup> M. Onoda and N. Naoto, J. Phys. Soc. Jpn. **71**, 19 (2002).
  - <sup>5</sup> T. Jungwirth, Q. Niu, and A. H. MacDonald, Phys. Rev. Lett. **88**, 207208 (2002).
  - <sup>6</sup> S. Fujimoto, Phys. Rev. B **77**, 220501 (2008).
  - <sup>7</sup> C. Zhang, S. Tewari, R. M. Lutchyn, and S. Das Sarma, Phys. Rev. Lett. **101**, 160401 (2008).
  - <sup>8</sup> C. Richter *et al.*, Nature **502**, 528 (2013), Letter.
  - <sup>9</sup> A. D. Caviglia *et al.*, Nature **456**, 624 (2008).
  - <sup>10</sup> P. B. Allen *et al.*, Phys. Rev. B **53**, 4393 (1996).
  - <sup>11</sup> Y. Kats, I. Genish, L. Klein, J. W. Reiner, and M. R. Beasley, Phys. Rev. B **70**, 180407 (2004).
  - <sup>12</sup> M. Izumi, K. Nakazawa, Y. Bando, Y. Yoneda, and H. Terachi, J. Phys. Soc. Jpn. **66**, 3893 (1997).
  - <sup>13</sup> R. Mathieu *et al.*, Phys. Rev. Lett. **93**, 016602 (2004).
  - <sup>14</sup> K. Oda *et al.*, J. Phys. Soc. Jpn. **70**, 2999 (2001).
  - <sup>15</sup> W.-L. Lee, S. Watauchi, V. L. Miller, R. J. Cava, and N. P. Ong, Science **303**, 1647 (2004).
  - <sup>16</sup> I. Galanakis, P. H. Dederichs, and N. Papanikolaou, Phys. Rev. B **66**, 174429 (2002).
  - <sup>17</sup> T. Block, M. J. Carey, B. A. Gurney, and O. Jepsen, Phys. Rev. B **70**, 205114 (2004).
  - <sup>18</sup> J. G. Checkelsky, M. Lee, E. Morosan, R. J. Cava, and N. P. Ong, Phys. Rev. B **77**, 014433 (2008).
  - <sup>19</sup> R. Karplus and J. M. Luttinger, Phys. Rev. **95**, 1154 (1954).
  - <sup>20</sup> L. Berger, Phys. Rev. B **2**, 4559 (1970).
  - <sup>21</sup> J. Smit, Physica **21**, 877 (1955).
  - <sup>22</sup> S. Onoda, N. Sugimoto, and N. Nagaosa, Phys. Rev. Lett. **97**, 126602 (2006).
  - <sup>23</sup> Y. A. Bychkov and E. I. Rashba, Journal of Physics C: Solid State Physics **17**, 6039 (1984).
  - <sup>24</sup> V. K. Dugaev, P. Bruno, M. Taillefumier, B. Canals, and C. Lacroix, Phys. Rev. B **71**, 224423 (2005).
  - <sup>25</sup> H. Kontani, J. Goryo, and D. S. Hirashima, Phys. Rev. Lett. **102**, 086602 (2009).
  - <sup>26</sup> D. Culcer, A. MacDonald, and Q. Niu, Phys. Rev. B **68**, 045327 (2003).
  - <sup>27</sup> J. Alicea, Phys. Rev. B **81**, 125318 (2010).
  - <sup>28</sup> P. Anderson, Journal of Physics and Chemistry of Solids **11**, 26 (1959).
  - <sup>29</sup> Y. Dubi, Y. Meir, and Y. Avishai, Nature **449**, 876 (2007).
  - <sup>30</sup> N. Mohanta and A. Taraphder, J Phys: Condens Matter **26**, 025705 (2014); *ibid*, **26**, 215703 (2014).
  - <sup>31</sup> A. C. Potter and P. A. Lee, Phys. Rev. B **83**, 184520 (2011).